Available online at www.sciencedirect.com
ScienceDirect
Energy Conversion and Management 48 (2007) 454–461
ENERGY CONVERSION & MANAGEMENT
www.elsevier.com/locate/enconman

A potential flow 2-D vortex panel model: Applications to vertical axis straight blade tidal turbine

L.B. Wang *, L. Zhang, N.D. Zeng

School of Shipbuilding Engineering, Harbin Engineering University, No. 145 Nantong Street, NanGang District, Harbin, Heilongjiang Province 150001, PR China

Received 17 December 2005; accepted 26 June 2006
Available online 22 August 2006

Abstract

A potential flow 2-D vortex panel model (VPM2D) for unsteady hydrodynamics calculation of the vertical axis straight blade variable pitch turbine was given for tidal streams energy conversion. Numerical results of predicted instantaneous blade forces and wake flow of the rotor showed good agreement with the test data. The model was also compared with the previous classic free vortex model (V-DART) and vortex method combined with finite element analysis (FEVDTM). It showed that the present model was much better than the former, less complex than the latter and suitable for designing and optimization of the vertical axis straight blade turbine.

Keywords: Tidal streams energy; Vertical axis turbine; Hydrodynamic performance; Vortex panel method; Potential flow theory

1. Introduction

Since 1970, several fluid dynamic prediction models have been formulated for vertical axis turbines such as the Darrieus turbine. These models can be classified as two families according to their theory basis: the stream tube modeling method, which is based upon equating the forces on the rotor blade to the change in streamwise momentum through the rotor; and the vortex modeling method, which is based upon vortex representations of the blades and their wakes.

The stream tube approach needs much less computation time, but the vortex approach is more accurate. Stream tube models such as the *Single Stream-Tube Model* proposed by Templin [1], the Multiple Stream-Tube Model by Strickland [2], the Double-Multiple Stream-Tube Model by Paraschivoiu [3] and the Stream-Tube Model with modification by Zhang et al. [4] can predict effectively the general performance of the rotor (power coefficient vs. tip to speed ratio, etc.); and their relatively low computational cost makes them a useful practical tool for design. On the other hand, they exhibit difficulties in predicting the instantaneous forces on the blades and the details of the flow field, but all these informations are important to the improvement and optimal design of the turbine. In order to calculate these forces in detail and accurately, vortex models have to be used. In the present paper, a potential flow 2-D vortex panel model is formulated and compared with the previous classic free vortex model (V-DART) proposed by Strickland et al. [5] and the vortex method combined with finite element analysis (FEVDTM) proposed by Ponta and Jacovkis [6]. The idea is to find a sufficiently accurate and much less sophisticated model.

2. Previous vortex models

2.1. Free vortex model

Several free vortex models for vertical-axis wind turbines have been developed in the past such as those due to Fanucci and Walters [7], Wilson [8], Holmes [9] and Strickland et al. [5]. They are based upon replacement of the rotor blade by a bound vortex filament (or several

* Corresponding author.
E-mail address: lubingwang@hotmail.com (L.B. Wang).

0196-8904/$ - see front matter © 2006 Elsevier Ltd. All rights reserved.
doi:10.1016/j.enconman.2006.06.017

filaments) called a lifting line that changes its strength as a function of the azimuthal position. In these methods, the V-DART model [5] is the most popular. This model requires that every rotor blade be divided into a number of segments along its span. Every segment is represented by a bound vortex filament (a lifting line) positioned along the camber line. Because of the bound vortex variation, spanwise vortices are shed, and their strengths are equal to the change of the bound vortex strength. Thus, the wake is modeled by a discrete set of free vortex filaments shed from each blade element in such a way as to satisfy Kelvin's theorem:

$$\Gamma_{\mathrm{w}}^{(k)} + \Gamma_{\mathrm{f}}^{(k)} = \Gamma_{\mathrm{f}}^{(k-1)} \tag{1}$$

where $\Gamma_{\mathrm{w}}^{(k)}$ is the strength of the vortex shed at the kth iteration, $\Gamma_{\mathrm{f}}^{(k)}$ is the bound vortex strength at the kth iteration and $\Gamma_{\mathrm{f}}^{(k-1)}$ is the bound vortex strength at the $(k-1)$th iteration. A simple representation of this vortex system associated with a blade element is shown in Fig. 1.

In order to allow closure of the proposed vortex model, a relation between the bound vortex strength Γ_{f} and the local flow velocity at the blade must be obtained. Up to the present, several techniques have been developed to achieve this. One of the most successful is as follows:

$$\Gamma_{\mathrm{f}} = \frac{1}{2} C_{\mathrm{L}} C V_{\mathrm{R}} \tag{2}$$

Here, C_{L} is the foil section lift coefficient, C is the blade chord length and V_{R} is the local relative fluid velocity. The lift per unit span on a blade segment can be given by the Kutta–Joukowski law in terms of the bound vortex strength Γ_{f}; and the lift can also be formulated in terms of the airfoil section lift coefficient. Equating these two expressions for lift yields the required relationship at a particular blade segment.

The free vortex model has several advantages over the previous methods. There are, however, shortcomings of this approach too. The required airfoil section lift coefficients are taken from static test data for their use, but the circulation about a pitching airfoil moving over a curvilinear path differs from those found on non-pitching, non-rotating sections. The surface pressure distribution differs too, and it would alter the boundary layer structure and, therefore, the fluid dynamic characteristics. So, the Kutta condition may be poorly matched and the calculated forces not sufficiently accurate.

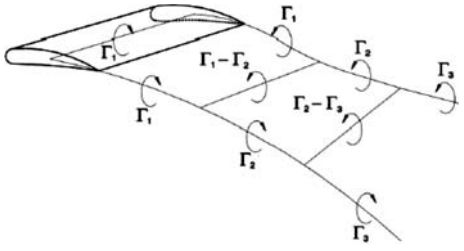

Fig. 1. Vortex structure for single blade element of V-DART model.

2.2. Free vortex model combined with finite element analysis

In order to avoiding some remaining deficiencies in the classic free vortex models, Ponta and Jacovkis presented the FEVDTM model combining the free vortex model with a finite element analysis of the flow in the surroundings of the blades [6]. The free vortex method acts as a macro-model whose results are used as a boundary condition on the boundary of the finite element analysis area, which acts as a micro-model (see Fig. 2). The bound vortex strength is determined by integration of the flow velocity field obtained from the finite element analysis. This sequence defines an iterative scheme; and after it converges, the surface pressure distribution over the foil can be calculated by integrating the momentum equation. From this knowledge of the pressure and velocity distributions, a boundary layer model to calculate the viscous shear stress over the foil surface is applied. The fluid dynamic forces on the blade are determined by integration of these pressure and shear stress distributions.

This model is a fully theoretical tool because it does not use airfoil test data. Moreover, it includes the rotational effect induced by turbine rotation, so that it does not suffer from the irrotational flow condition of potential analysis, and therefore, it allows improving the accuracy of prediction.

3. Two-dimensional vortex panel model (VPM2D)

The purpose of the present paper is to show a 2-D vortex panel method (VPM2D) for modeling the vertical axis straight blade turbine. The method is based on the surface distribution of singularity elements to fulfill the boundary conditions on the actual surfaces of turbine blades. In detail, discrete source elements are distributed along the blade section contour with discrete vortex elements along the camber line; and a wake model is established by the distribution of discrete concentrated vortices on the wake shedding lines. The Kutta condition is realized by forcing the pressure difference at the trailing edge (TE) between the suction and pressure sides to approach zero. The time stepping method is applied to get the strength of each singularity element and the velocity distribution along the blade section contour. The fluid dynamic pressures and

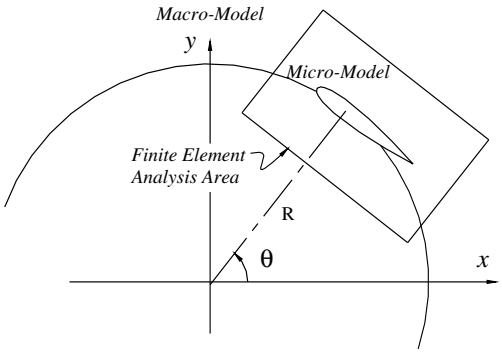

Fig. 2. Finite element analysis area and macro-model area for FEVDTM.

the loads generated by the blade can be calculated by using the unsteady Bernoulli's equation.

3.1. Theoretical background

As shown in Fig. 3, the origin of an inertial frame of reference (X, Y) is selected to coincide with the center axis of the turbine with the X axis direction coinciding with the free stream velocity $\boldsymbol{V}_\infty$. A body fixed coordinate system (x, y) is built on one of the blades with the x axis pointing to the trailing edge along the chord line. The motion of the blade is assumed to be known and can be defined in the inertial frame of reference by the velocity $\boldsymbol{U}$ which is the motion of the center of the body fixed system, and the angular velocity $\boldsymbol{\Omega}$ which is the rotation rate of the body fixed reference system as shown in Fig. 4.

The fluid surrounding the blades is assumed to be inviscid, irrotational and incompressible in the entire flow field, excluding the solid boundaries S_b and the wakes S_w of the blades. So, the perturbation velocity potential ϕ formulated in the body fixed system (x, y) satisfies:

$$\nabla^2\phi(x,y,t) = 0 \quad \text{(in fluid)} \tag{3}$$

The time dependent boundary condition requiring zero flow across the surface is:

$$\nabla\phi\cdot\boldsymbol{n} = (\boldsymbol{U} - \boldsymbol{V}_\infty + \boldsymbol{\Omega}\times\boldsymbol{r})\cdot\boldsymbol{n} \quad \text{(on the blade surfaces)} \tag{4}$$

Here, $\boldsymbol{r}$ is the position vector and $\boldsymbol{n}$ is the normal to the surface of the solid boundaries.

The second boundary condition requires that the flow disturbance due to the turbine's motion through the fluid should diminish far from the turbine

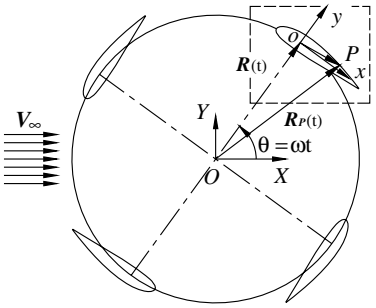

Fig. 3. Reference coordinate system for VPM2D model.

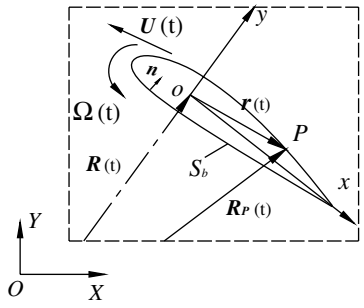

Fig. 4. Body-fixed coordinate system for VPM2D model.

$$\nabla\phi \to 0 \text{ (at infinity)} \tag{5}$$

and the initial disturbance is zero,

$$\nabla\phi \to 0 \ (t = 0) \tag{6}$$

The Kutta condition is necessary to make this lifting flow problem unique by applying equal pressures at the up and down sides of the blade section trailing edge:

$$p_u = p_d \quad \text{(at the TE)} \tag{7}$$

The pressure follows from the unsteady Bernoulli's equation, namely

$$\frac{p - p_\infty}{\rho} = -\frac{\partial\phi}{\partial t} + (\boldsymbol{U} - \boldsymbol{V}_\infty + \boldsymbol{\Omega}\times\boldsymbol{r})\cdot\nabla\phi - \frac{1}{2}(\nabla\phi)^2 \tag{8}$$

So Eq. (7) can be expressed as:

$$\begin{aligned}\frac{p_u - p_d}{\rho} &= \frac{\partial\phi_d}{\partial t} - \frac{\partial\phi_u}{\partial t} + (\boldsymbol{U} - \boldsymbol{V}_A + \boldsymbol{\Omega}\times\boldsymbol{r}_u)\cdot\nabla\phi_u \\ &\quad - (\boldsymbol{U} - \boldsymbol{V}_A + \boldsymbol{\Omega}\times\boldsymbol{r}_d)\cdot\nabla\phi_d + \frac{1}{2}(\nabla\phi_d)^2 \\ &\quad - \frac{1}{2}(\nabla\phi_u)^2 \\ &= 0\end{aligned} \tag{9}$$

If the up and down sides of the trailing edge are very close to each other, then it will suffice to write:

$$\boldsymbol{r}_u \approx \boldsymbol{r}_d \approx \frac{1}{2}(\boldsymbol{r}_u + \boldsymbol{r}_d) = \bar{\boldsymbol{r}}_{TE} \tag{10}$$

So Eq. (8) can be simplified as:

$$\begin{aligned}\frac{\partial(\phi_u - \phi_d)}{\partial t} &= \frac{\partial\Gamma_f}{\partial t} \approx (\boldsymbol{U} - \boldsymbol{V}_A + \boldsymbol{\Omega}\times\bar{\boldsymbol{r}}_{TE})\cdot(\nabla\phi_u - \nabla\phi_d) \\ &\quad + \frac{1}{2}(\nabla\phi_d - \nabla\phi_u)\cdot(\nabla\phi_d + \nabla\phi_u) \\ &= (\boldsymbol{U} - \boldsymbol{V}_A + \boldsymbol{\Omega}\times\bar{\boldsymbol{r}}_{TE} - \overline{\boldsymbol{V}}_{TE})\cdot(\nabla\phi_u - \nabla\phi_d)\end{aligned} \tag{11}$$

where $\overline{\boldsymbol{V}}_{TE} = \frac{1}{2}(\nabla\phi_d + \nabla\phi_u)$.

For the unsteady case, the Kelvin condition will supply an additional equation that can be used with the Kutta condition to determine the streamwise strength of the vorticity shed into the wake. In general, this condition can be expressed as:

$$\frac{d\Gamma_{Total}}{dt} = \frac{d(\Gamma_f + \Gamma_w)}{dt} = 0 \text{ (for any } t) \tag{12}$$

or

$$\frac{\partial\Gamma_f}{\partial t} = -\frac{\partial\Gamma_w}{\partial t} \approx -\frac{\Gamma_w^{(k)} - \Gamma_w^{(k-1)}}{\Delta t} = -\frac{\gamma_w^{(k)}}{\Delta t} \quad \text{and} \quad \Gamma_f^{(k)} + \gamma_w^{(k)} \approx \Gamma_f^{(k-1)} \tag{13}$$

3.2. Numerical model

Because the turbine undergoes a time dependent motion that starts at $t = 0$, the solution can be calculated at successive intervals of time:

$$t_k \qquad (t_0 = 0, \quad k = 1, 2, 3, \ldots) \tag{14}$$

At time t_k, the section contour and the chord line of every blade are, respectively, replaced by n and m straight line elements (see Fig. 5). To the pth blade ($p = 1, \ldots, Z$), a uniform source distribution $\sigma_{i,p}^{(k)}$ is placed on the ith element ($i = 1, \ldots, n$) of the section contour with a uniform vorticity distribution $\gamma_{\mathrm{f},p}^{(k)}$ on each chord element, where the superscript (k) refers to the time t_k, the subscript p to the pth blade and Z to the blade number of the turbine. If the chord line length is $C_{\mathrm{f},p}$, the overall circulation of the pth blade $\Gamma_{\mathrm{f},p}^{(k)}$ equals $\gamma_{\mathrm{f},p}^{(k)} \cdot C_{\mathrm{f},p}$. The vorticity on the trailing edge wake $\gamma_{\mathrm{w},p}^{(k)}$ is modeled by the discrete concentrated vortex for every blade, and from Eq. (13), it satisfies

$$\gamma_{\mathrm{w},p}^{(k)} = \Gamma_{\mathrm{f},p}^{(k-1)} - \Gamma_{\mathrm{f},p}^{(k)} \tag{15}$$

Thus, the circulation of this vortex is the change of that around the blade between times t_{k-1} and t_k, assuming that $\Gamma_{\mathrm{f},p}^{(k-1)}$ has already been evaluated. It is assumed further to be convected from the trailing edge with the velocity of that point, so its position can be calculated as:

$$\boldsymbol{r}_{\mathrm{w},p}^{(k)} = \bar{\boldsymbol{r}}_{\mathrm{TE},p} - \beta\left(\boldsymbol{U}_p - \boldsymbol{V}_\infty + \boldsymbol{\Omega}_p \times \bar{\boldsymbol{r}}_{\mathrm{TE},p} - \overline{\boldsymbol{V}}_{\mathrm{TE},p}\right)\Delta t \tag{16}$$

Here, β is the position coefficient of the newly shedding vortex. In the present calculation, $\beta = 0.5$ is assumed.

The downstream wake is formed by discrete concentrated vortices from the vorticity shed at earlier time intervals. Each of these vortices is assumed to be convected according to the resultant velocity calculated at the center of itself at each successive time interval. Thus, the pattern of the downstream discrete vortices, their strengths and their positions are regarded as known at time t_k.

Now, the velocity potential ϕ can be constructed by summing up the basic solutions of the source and vorticity distributions over the solid contours, chord lines and wakes of the blades. Thus, at time t_k, there are $(n+2) \cdot Z$ total unknowns: $\sigma_{i,p}$, $\gamma_{\mathrm{f},p}$ and $\gamma_{\mathrm{w},p}^{(k)}$ ($i = 1, 2, \ldots, n$; $p = 1, 2, \ldots, Z$). The basic equation systems can be formulated as follows (noting that, for briefness, the superscript k is omitted if not leading to misunderstanding).

1. From Eq. (4), there are $n \cdot Z$ equations for the conditions of zero normal flow at the midpoint of each blade section contour panel:

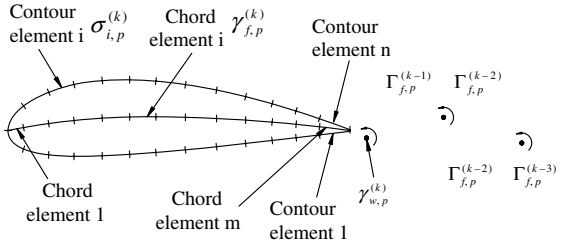

Fig. 5. Model for the pth blade at time t_k.

$$\sum_{q=1}^{Z}\left[\left(\sum_{j=1}^{n} A_{ip,jq}\sigma_{j,q}\right) + A_{ip,(n+1)q}\gamma_{\mathrm{f},q} + \left(\sum_{j=1}^{k} C_{ip,jq}\gamma_{\mathrm{w},q}^{(j)}\right)\right] = \boldsymbol{n}_{ip} \cdot (\boldsymbol{U}_p - \boldsymbol{V}_\infty + \boldsymbol{\Omega}_p \times \boldsymbol{r}_{ip}) \quad (i = 1, 2, \ldots, n; \quad p = 1, 2, \ldots, Z) \tag{17}$$

2. From Eq. (11) there are Z equations for Kutta conditions:

$$\sum_{q=1}^{Z}\left[\left(\sum_{j=1}^{n} A_{(n+1)p,jq}\sigma_{j,q}\right) + A_{(n+1)p,(n+1)q}\gamma_{\mathrm{f},q} + \left(\sum_{j=1}^{k} C_{(N+1)p,jq}\gamma_{\mathrm{w},q}^{(j)}\right)\right] = -\frac{\gamma_{\mathrm{w},p}^{(k)}}{\Delta t} \tag{18}$$

3. From Eq. (13), there are Z equations for Kelvin conditions:

$$C_{\mathrm{f},p} \cdot \gamma_{\mathrm{f},p}^{(k)} + \gamma_{\mathrm{w},p}^{(k)} = C_{\mathrm{f},p} \cdot \gamma_{\mathrm{f},p}^{(k-1)} \tag{19}$$

where $i = 1, 2, \ldots, n$ and $p = 1, 2, \ldots, Z$ and $A_{ip,jq}$ and $C_{ip,jq}$ are appropriate influence coefficients, which depend on the instantaneous coordinates of the relevant panel elements.

3.3. Method of solution

Now the solution will be unique. However, the equation system defined by Eqs. (17)–(19) is nonlinear, so an iterative scheme is needed. At the beginning of each time step, an initial value is given to $\overline{\boldsymbol{V}}_{\mathrm{TE},p}$ (e.g. zero) to linearize the equation system, and the unknowns can be solved. Then, a new value of $\overline{\boldsymbol{V}}_{\mathrm{TE},p}$ can be calculated with the new solved unknowns. After that, recalculate the equation system by introduce this newly solved $\overline{\boldsymbol{V}}_{\mathrm{TE},p}$ to get the new results of the unknowns. Continue this iterative process until it converges.

Calculating shows that using the last time interval's converged value of $\overline{\boldsymbol{V}}_{\mathrm{TE},p}$ as the initial value of the present time interval will accelerate the iterative process; i.e. setting

$$\overline{\boldsymbol{V}}_{\mathrm{TE},p0}^{(k)} = \overline{\boldsymbol{V}}_{\mathrm{TE},p}^{(k-1)} \tag{20}$$

where $\overline{\boldsymbol{V}}_{\mathrm{TE},p0}^{(k)}$ is the iterative initial value at time t_k and $\overline{\boldsymbol{V}}_{\mathrm{TE},p}^{(k-1)}$ is the converged value at time t_{k-1}.

Once the source and vorticity strengths have been determined, the velocity distribution over the blade sections can be calculated. The velocity potential ϕ is obtained by integrating the velocity field along the blade section contour from the down side to the upside of the blade trailing edge.

$$\phi(q) = \phi_0 + \int_{q_1}^{q} \boldsymbol{V} \cdot \mathrm{d}\boldsymbol{l} \tag{21}$$

Here, $\phi_0 = \phi(q_1)$ is the velocity potential at the down side of the trailing edge.

The value of $\partial\phi/\partial t$ at the midpoint of the ith element of the pth blade at time t_k is approximated by

$$\left.\frac{\partial\phi}{\partial t}\right|_{ip}^{(k)} = \frac{\phi_{ip}^{(k)} - \phi_{ip}^{(k-1)}}{t_k - t_{k-1}} \quad (i = 1, 2, \ldots, n; \ p = 1, \ldots, Z) \tag{22}$$

The pressure can be calculated by applying the unsteady Bernoulli's equation as in Eq. (8), and the pressure coefficient on the single blade is defined as:

$$C_p = \frac{p - p_\infty}{0.5\rho V_\infty^2} \tag{23}$$

The force on the blade can be expressed as:

$$\boldsymbol{F} = (F_x, F_y) = 0.5\rho V_{\mathrm{A}}^2 \cdot \int_{S_{\mathrm{b}}} C_p \boldsymbol{n}\,\mathrm{d}S \tag{24}$$

Once the solution at time t_k has been determined, the model is set up for the time t_{k+1}. Every discrete concentrated vortex of each blade is assumed to move at the local velocity of the center of itself, namely

$$\boldsymbol{r}_{\mathrm{w},p}^{(i+1)} = \boldsymbol{r}_{\mathrm{w},p}^{(i)} + (t_{k+1} - t_k) \cdot \boldsymbol{V}_{\mathrm{w},p}^{(i)} \quad (i = 1, 2, \ldots, k; \quad p = 1, \ldots, Z) \tag{25}$$

Here, $\boldsymbol{r}_{\mathrm{w},p}^{(i)}$ is the position vector to the center of the pth blade's ith wake vortex, $\boldsymbol{V}_{\mathrm{w},p}^{(i)}$ is the total velocity of that point at time t_k and the strengths of the wake vortices are assumed to remain unchanged.

Additional consideration must be paid to the blade vortex interaction. If a vortex can impinge on the blade, its trajectory needs to be regulated. The criterion is based on the principle that the vortex can at most slide along the blade surface. Here, the method of Yao and Liu [10] is referenced. If the predicted position of the vortex is in the blade, the new position must be corrected by modifying Eq. (25) as follows:

$$\boldsymbol{r}_{\mathrm{w},p}^{(i+1)} = \boldsymbol{r}_{\mathrm{w},p}^{(i)} + (t_{k+1} - t_k) \cdot \left|\boldsymbol{V}_{\mathrm{w},p}^{(i)}\right| \cdot \boldsymbol{l} \tag{26}$$

Here, $\boldsymbol{l}$ is the unit tangential vector at the predicted impinging location on the blade surface.

In present model, a correction method based on the Von Karman integral momentum equation for the boundary layer is applied in order to calculate the viscous forces after the potential flow computation. It can be expressed as:

$$\frac{\mathrm{d}\delta}{\mathrm{d}\xi} = \frac{15}{2U_{\mathrm{e}}}\left[\frac{2\nu}{\delta} - \frac{3}{5}\delta\frac{\mathrm{d}U_{\mathrm{e}}}{\mathrm{d}\xi}\right], \quad \delta|_{\xi=0} = 0 \tag{27}$$

where δ is the boundary layer thickness, U_{e} is the velocity on the boundary layer external border and is known after the potential flow calculation, ξ is the coordinate along the blade section contour and ν is the kinematic viscosity coefficient. The fourth order Runge–Kutta algorithm is used to solve this problem by assuming a quadratic velocity profile inside the boundary layer. Then, the shear stress τ_{w} on the blade section contour is calculated by

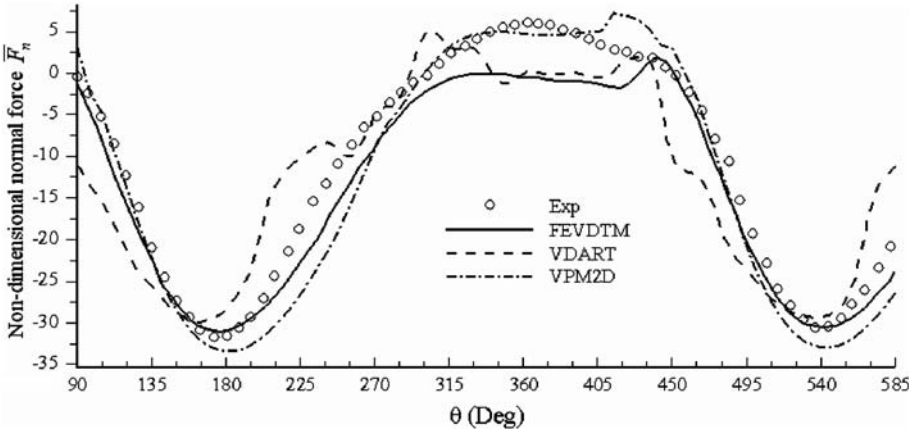

Fig. 6. Comparison of non-dimensional normal force against azimuthal angle.

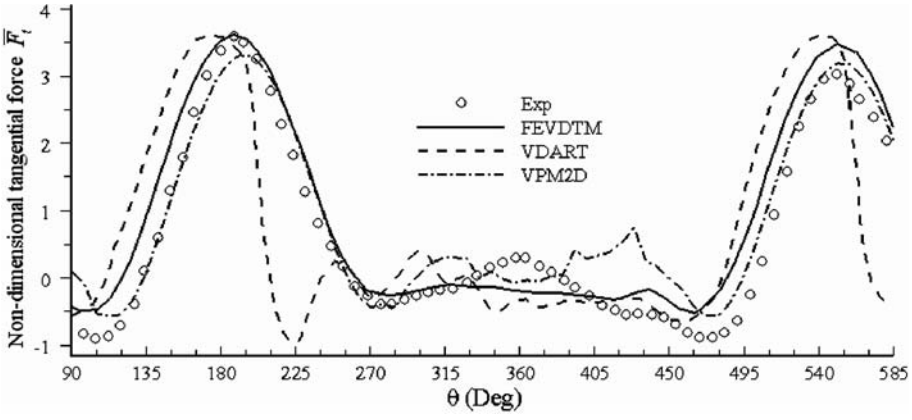

Fig. 7. Comparison of non-dimensional tangential force against azimuthal angle.

$$\tau_w = \frac{2\mu U_e}{\delta} \tag{28}$$

Here, μ is the dynamic viscosity coefficient. At last, the shear stresses are integrated along the foil contour to obtain the total viscous force actuating on the blades.

4. Validation of the VPM2D model

In the present part, the VPM2D model will be applied to an example of Strickland et al. [5] (also included by Klimas [11] and re-simulated by Ponta and Jacovkis [6]). This example is based on an experimental test over a NACA 0012 straight bladed rotor with 1, 2 or 3 blades. The wake vorticity visualizations were recorded for all three blades; but the normal and tangential forces acting on the blade were measured only in terms of the two bladed rotor.

The test was made at a tip to speed ratio $\lambda = \omega R/V_\infty = 5.0$, the blade chord length Reynolds' number $Re = CV_\infty/v = 40{,}000$ and the chord radius ratio $C/R = 0.15$. Here, R is the rotor's radius and ω is the rotor's angular velocity.

The lift and drag coefficients of the blade section are, respectively, defined as:

$$C_L = \frac{L}{0.5\rho V_R^2 C}, \quad C_D = \frac{D_r}{0.5\rho V_R^2 C} \tag{29}$$

Here, L and D_r are, respectively, the lift and drag on the blade section, ρ is the fluid density and V_R is the relative velocity of the blade. They can be expressed as:

$$L = F_y \cos\alpha - F_x \sin\alpha \tag{30}$$

$$D_r = F_x \cos\alpha + F_y \sin\alpha \tag{31}$$

$$V_R = \sqrt{(R\omega\cos\theta)^2 + (V_\infty + R\omega\sin\theta)^2} \tag{32}$$

where $\theta = \omega t$ is the azimuthal angle as shown in Fig. 3; α is the blade section angle of attack

$$\alpha = \arctan\frac{V_\infty\cos\theta}{V_\infty\sin\theta + R\omega} = \arctan\frac{\cos\theta}{\sin\theta + \lambda} \tag{33}$$

The non-dimensional tangential force $\overline{F}_t$ and normal force $\overline{F}_n$ of the blade section are defined as follows:

$$\overline{F}_t = \frac{F_t}{0.5\rho V_\infty^2 C} = C_t\left(\frac{V_R}{V_\infty}\right)^2 \tag{34}$$

$$\overline{F}_n = \frac{F_n}{0.5\rho V_\infty^2 C} = C_n\left(\frac{V_R}{V_\infty}\right)^2 \tag{35}$$

C_t and C_n have relations to the foil lift and drag coefficients as follows:

$$C_t = C_L\sin\alpha - C_D\cos\alpha \tag{36}$$

$$C_n = C_L\cos\alpha + C_D\sin\alpha \tag{37}$$

The calculated results of the VPM2D model will be compared with those of the V-DART model, FEVDTM model and experiment. Fig. 6 shows this comparison of the non-dimensional normal force $\overline{F}_n$ against the azimuthal angle θ starting from $\theta_0 = 90°$, while Fig. 7 shows the non-dimensional tangential force case.

In the experiment of Strickland et al. [5], the wake's conformation was studied by dye injection through the trailing edge of one of the rotor's blades. This streak line

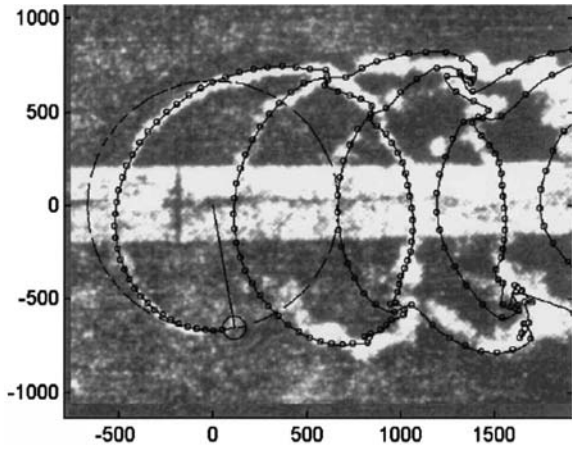

Fig. 8. Wake vortex centers path of experimental visualization superimposed over by FEVDTM prediction (one blade rotor).

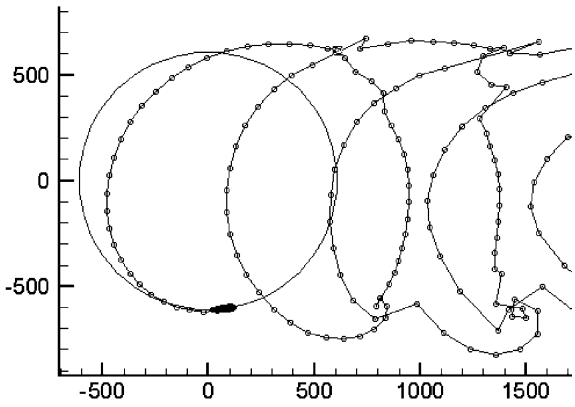

Fig. 9. Wake vortex centers path of VPM2D prediction (one blade rotor).

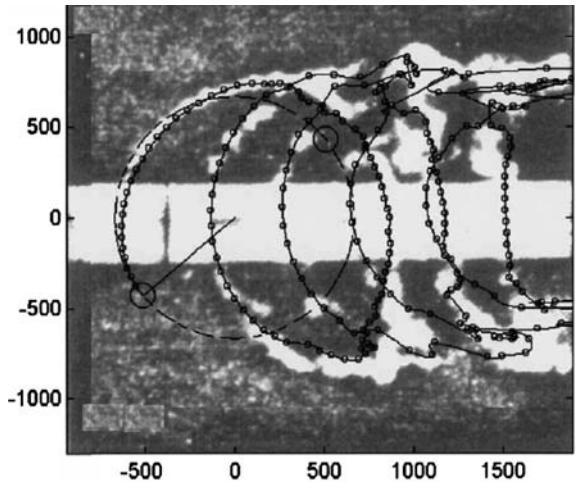

Fig. 10. Wake vortex centers path of experimental visualization superimposed over by FEVDTM prediction (two blade rotor).

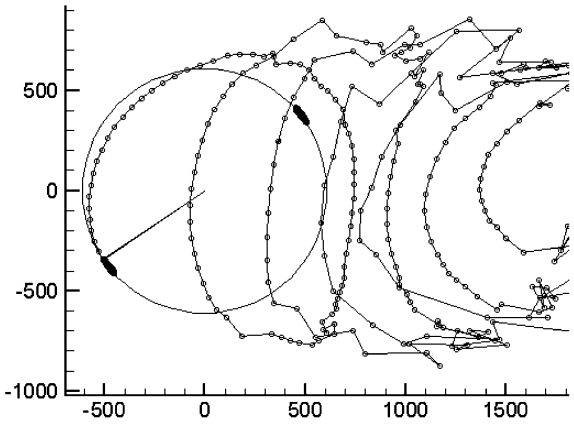

Fig. 11. Wake vortex centers path of VPM2D prediction (two blade rotor).

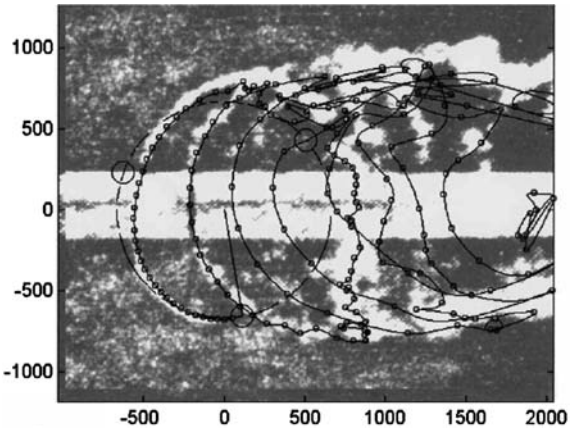

Fig. 12. Wake vortex centers path of experimental visualization superimposed over by FEVDTM prediction (three blade rotor).

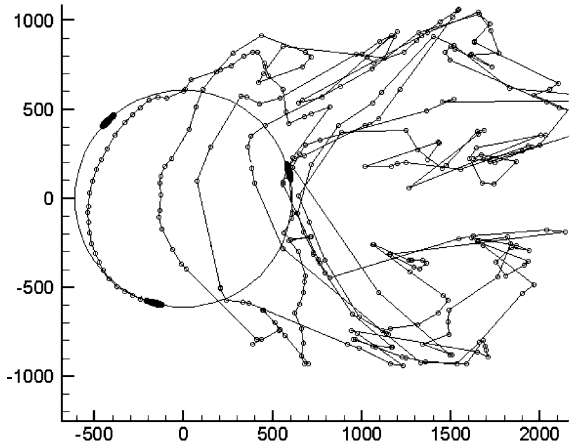

Fig. 13. Wake vortex centers path of VPM2D prediction (three blade rotor).

is indicative of the vortex sheet produced by the foil or it can be conceived as a line made up of shed vortex centers. Figs. 8–13 show, respectively, the comparison for these three cases of 1, 2 and 3 blades of the VPM2D prediction, the FEVDTM prediction and the experimental visualization (noting that the FEVDTM prediction and the experimental visualization are superimposed together in the plots).

5. Conclusions

The VPM2D model prediction results in Figs. 6 and 7 show good agreement with the experiment data when predicting instantaneous blade forces. From the comparisons, it can be seen clearly that these results are better than those of the V-DART model and no worse than those of the FEVDTM model, and the VPM2D model has the advantage of simpleness and requiring less computer processing time.

From these plots, it is apparent that the non-dimensional tangential and normal forces on the blade in the upstream region are much greater than those in the downstream region. As might be expected, the minimum value of $\overline{F}_t$ and the zero value of $\overline{F}_n$ occur at azimuthal angles greater than 90° instead of 90°. In the upstream region, $\overline{F}_t$ and $\overline{F}_n$ are not symmetrical about an azimuthal angle of 180°, the same occurring in the downstream region at the angle of 360°. These phenomena occur because of the blade–blade and vortex–blade interactions and the induced lateral flow velocity, and the prediction of these characteristics is the advantage of the vortex method over the stream tube method.

Figs. 8–13 show comparisons of the wake vorticity streak lines for one blade, two blade and three blade rotors, respectively. The comparison between the two models' predicted and experimental results show good agreement too. The increase in blockage and interaction with increasing turbine solidity is clearly seen.

From the above comparisons and analyses, the validation of the VPM2D model should be assured in some respects. This model is more accurate than the V-DART model and simpler and needs less CPU time than the FEVDTM model. Thus, it can be used for performance prediction and design of the vertical axis straight blade turbine, especially for the optimal design of the turbine through appropriate choice of the blade pitching method because it automatically includes the rotational effect of the blade around the axis of itself [see Eq. (17)].

However, this model does not include consideration of the phenomenon of dynamic stall, which often occurs at low tip to speed ratio and high turbine solidity conditions, and it can only focus on the 2-D problem (straight blade turbine with big foil span to chord ratio). So the VPM2D model is a fully theoretical tool that could be used as the basis of a future more sophisticated model that includes theoretical stall and three-dimensional simulation.

Acknowledgements

The authors gratefully acknowledge the financial supports by the National Natural Science Foundation of China through Grant 50279004 and the National Hi-Tech. R&D Program of China through Grant 2002AA516010.

References

[1] Templin RJ. Aerodynamic performance theory for the NRC vertical axis wind turbine. NRC of Canada TR, LTR-LA-160; 1974.
[2] Strickland JH. The Darrieus turbine: a performance prediction model using multiple streamtubes. Sandia Laboratory Report SAND 75-041; 1975.
[3] Paraschivoiu I. Aerodynamic loads and performance of the Darrieus rotor. J Energy 1981;6(6):406–12.
[4] Zhang L, Wang LB, Li FL. Study on streamtube models for prediction of performance of vertical-axis variable-pitch turbine for tidal current energy conversion. J Harbin Eng Univ 2004;25(3): 261–266.
[5] Strickland JH, Webster BT, Nguyen T. A vortex model of the Darrieus turbine: an analytical and experimental study. Trans ASME J Fluids Eng 1979;101:500–5.
[6] Ponta FL, Jacovkis PM. A vortex model for Darrieus turbine using finite element techniques. Renew Energy 2001;24:1–18.
[7] Fanucci JB, Walters RE. Innovative wind machines: the theoretical performances of a vertical axis wind turbine. In: Proceedings of the vertical axis wind turbine technology workshop. Sandia Laboratory Report SAND 76-5586, May 1976: III-61-93.
[8] Wilson RE. Vortex sheet analysis of the Giromill. Trans ASME J Fluid Eng 1978;100(3):340–2.
[9] Holmes O. A contribution to the aerodynamic theory of the vertical axis wind turbine. In: Proceedings of the international symposium on wind energy systems, St. John's College, Cambridge England, September 1976: C4-55-72.
[10] Yao ZX, Liu DD. Vortex dynamics of blade–blade interaction. AIAA J 1998;36(3):497–504.
[11] Klimas PC. Darrieus rotor aerodynamics [J]. Trans ASME J Solar Energy Eng 1982;104:102–5.